

Non-Gaussian Chance-Constrained Trajectory Planning for Autonomous Vehicles in the Presence of Uncertain Agents

Allen Wang, Ashkan Jasour, and Brian C. Williams

Abstract—Agent behavior is arguably the greatest source of uncertainty in trajectory planning for autonomous vehicles. This problem has motivated significant amounts of work in the behavior prediction community on learning rich distributions of the future states and actions of agents. However, most current work in trajectory planning in the presence of uncertain agents or obstacles is limited to the case of Gaussian uncertainty, which is a limited representation, or requires sampling, which can be computationally intractable to encode in an optimization problem. In this paper, we present a general method for enforcing chance-constraints on the probability of collision with other agents in model predictive control problems for autonomous driving that can be used with non-Gaussian mixture models of agent positions. Our method involves using statistical moments of the non-Gaussian distributions to enforce Cantelli’s Inequality, which we show can upper bound the probability of collision. We then demonstrate its application to chance-constrained trajectory planning using model predictive contouring control. In experiments, we show that the resulting optimization problem can be solved with state-of-the-art nonlinear program (NLP) solvers to plan trajectories with 5 second horizons in real-time.

I. INTRODUCTION

In order for autonomous vehicles to drive safely on public roads, they need to plan trajectories that take into account predictions of future positions of other agents (e.g. human driven vehicles, pedestrians, cyclists). However, predictions are inherently uncertain, especially predictions of human behavior. This fact is motivating significant amounts of work in the behavior prediction community to develop methods that predict *distributions* of future agent states and actions, usually using a deep neural network (DNN). For example, [22] trains a conditional variational autoencoder (CVAE) to generate samples of possible future trajectories; the DNN in this case essentially becomes the distribution from which samples can be drawn. [6], [9], [15] learn Gaussian mixture models (GMMs) for the agents’ future positions to handle both uncertainty in high level decisions, which tends to be multi-modal, and uncertainty in execution, which tends to be continuous. To address the fact that DNNs can produce trajectories of agent state that are physically impossible, some works instead learn distributions of agent actions that can be propagated through physical models [7], [30].

While work in behavior prediction can now generate rich distributions of future agent states and actions, most current works in chance-constrained trajectory planning only address the unimodal case and additionally either make Gaussian assumptions or require sampling [1]–[4], [23], [32], [36]. We

argue that handling non-Gaussian distributions is important because, for example, almost any distribution for agent action propagated through nonlinear dynamics models will result in non-Gaussian position distributions. Gaussians also have unbounded supports; this is unrealistic as the reachable set of agents is bounded by physical laws in reality. To handle non-Gaussian uncertainty, prior works generate n samples of the random variables and then perform n deterministic collision checks or enforce n deterministic constraints for each obstacle [3], [4]. This easily makes optimization computationally intractable because thousands of constraints need to be introduced to even enforce chance-constraints on the order of 10^{-2} for any practical problem [4]. Thus, we argue that it is important to develop non-sampling based methods that can handle mixtures of non-Gaussian distributions of agent positions in trajectory planning. To address non-Gaussian uncertainty in obstacle or agent positions without sampling, recent works on chance-constrained RRTs use a result from [5] that upper bounds the probability that an uncertain robot enters a half-space using the mean vector and covariance matrix of the robot position [29], [33]. This can be used to upper bound the probability of an uncertain robot entering a polytope by taking the bound corresponding to the least conservative half-space defining the polytope. For non-Gaussian uncertainty, sums-of-squares programming has been applied to the problem of trajectory tracking for nonlinear systems and risk assessment in the presence of non-convex obstacles, but current computational limitations restrict it to applications amenable to leveraging offline computation [17]–[19].

In this paper, we present a general chance-constrained model predictive control (cc-MPC) formulation for autonomous vehicles that can handle mixtures of non-Gaussian distributions of agent position. In contrast to the common confidence ellipse methods used to handle Gaussian uncertainty by inflating obstacles with ellipses, we instead draw an ellipse around the *ego vehicle* and upper bound the probability of an agent entering the ellipse using statistical moments of the distributions of the agent positions. Like the results of [29], [33], this method is also *distributionally robust* in the sense that the upper bound on risk is valid for all distributions with the given moments. It also has the added benefit of only upper bounding the probability mass inside an ellipse as opposed to the probability mass in a half-space. Since this approach only depends on statistical moments of the distributions, it can apply to non-Gaussian mixture models of future agent positions. It can even apply to the cases when DNNs are trained to generate samples of

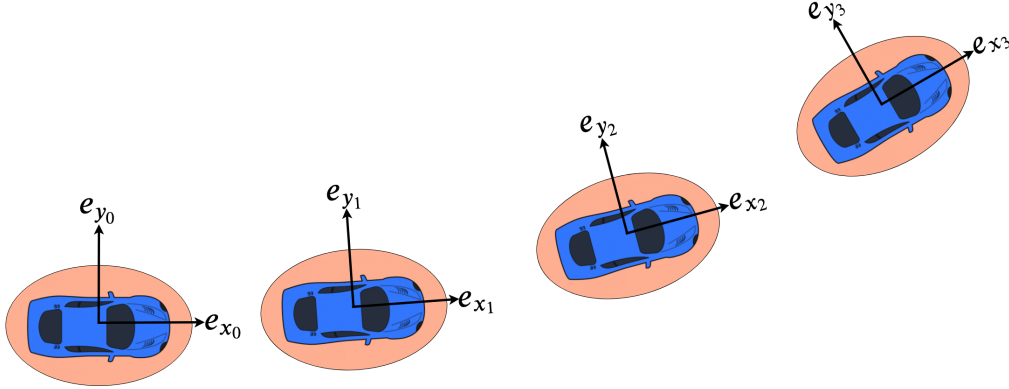


Fig. 1. A planned trajectory for the ego vehicle along with the “planned ego vehicle coordinates” and collision ellipses drawn around the vehicle.

trajectories, as statistical moments can be estimated from the generated samples; in essence, “compressing” a large number of samples into a small number of parameters. We then study the specific application of this formulation to trajectory planning using model predictive contouring control. In numerical experiments, we show how our formulation, when solved with advanced interior-point methods, can be used to plan trajectories with horizons of 5 seconds in real-time.

II. NOTATION

We adopt multi-index notation, so for any $\mathbf{x} \in \mathbb{R}^n$ and $\alpha \in \mathbb{N}^n$, $\mathbf{x}^\alpha = \prod_{i=1}^n x_i^{\alpha_i}$. Let $[n] = \{k \in \mathbb{N} : k \leq n\}$. Let \mathcal{S}_{++}^n denote the set of $n \times n$ positive definite matrices, and for any $Q \in \mathcal{S}_{++}^n$ and vector $\mathbf{x} \in \mathbb{R}^n$, let $Q(\mathbf{x}) = \mathbf{x}^T Q \mathbf{x}$. For any matrix Q , let Q_{ij} denote the element in the i th row and j th column. For any random vector \mathbf{w} , let $\mu_{\mathbf{w}}$ denote its mean vector and $\Sigma_{\mathbf{w}}$ denote its covariance matrix. Let $\mathbb{R}[\mathbf{x}]$ denote the ring of polynomials in \mathbf{x} over \mathbb{R} .

III. CC-MPC FORMULATION

A. Representation of Agent Predictions

We assume a behavior prediction system provides the distribution of future positions for an agent over a T step horizon, $\mathbf{a}_{1:T}$, in a fixed global coordinate system. The distributions can be either unimodal or a mixture of non-Gaussian random vectors. The distributions $\mathbf{a}_t = [a_{x_t}, a_{y_t}]^T$ are assumed to be either independent across time in the unimodal case or independent across time conditioned on a discrete mode in the mixture model case. This is a common assumption used in state of the art behavior prediction systems; thus, it does not significantly restrict our method’s range of applicability [6], [9], [30].

B. Definition of Risk

We define *risk* as the probability of an agent entering an ellipse around the ego vehicle. Ellipses can be fit relatively tightly to the profiles of vehicles which makes them a useful way to evaluate the probability of collision. To account for the fact that agents in the real world are not point masses, the ellipse should be scaled to account for the agent’s size. For

example, if a circle of radius r can be fit around the agent, then scaling the semi-major and semi-minor axes of the ego vehicle ellipse by r will account for the size of the agent¹. Multiple ellipses around the ego vehicle can also be defined if there are multiple agents in the environment of varying size. It is convenient to define the ellipse in a coordinate system affixed to a point on the ego vehicle; doing so allows the ellipse to be parameterized by a constant matrix $Q \in \mathcal{S}_{++}^2$. We will refer to the coordinates corresponding to the planned future poses of the ego vehicle as the “planned ego vehicle coordinates” and denote the agent positions in these planned coordinates as \mathbf{a}_t^* . For example, \mathbf{a}_3^* would be the position of the agent in the coordinate system defined by e_{x_3}, e_{y_3} in Figure 1. Thus, risk at each time step is defined as:

$$\mathbb{P}(Q(\mathbf{a}_t^*) \leq 1) \quad (1)$$

Note that $Q(\mathbf{a}_t^*)$ can be viewed as a random variable as measurable functions of random variables are still random variables (and similarly in the vector case). The risk along the entire planning horizon can be defined as:

$$\mathbb{P}\left(\bigcup_{t=1}^T \{Q(\mathbf{a}_t^*) \leq 1\}\right) \quad (2)$$

However, evaluating (2) without excessive conservatism is a non-trivial problem itself meriting a separate treatment. In this paper, we simply constrain the marginal probabilities at each time step, but we provide some discussion on existing methods for enforcing a constraint on (2).

C. Evaluating Risk Along a Trajectory

In general, the inclusion-exclusion principle exactly characterizes the risk along a trajectory in terms of the probabilities of intersections of the events:

$$(2) = \sum_{J \in \mathcal{P}([T])} (-1)^{|J|+1} \mathbb{P}\left(\bigcap_{j \in J} \{Q(\mathbf{a}_j^*) \leq 1\}\right) \quad (3)$$

¹We note that, in practice, this would work well for pedestrians and smaller vehicles, but not for semi-trucks.

Above, $\mathcal{P}(\cdot)$ denotes the power set operator and $|J|$ denotes the cardinality of the set J . In the case that the predictions \mathbf{a}_t are independent across time, the probability of the intersection of events can be computed as the product of the marginal probabilities, so only the marginal probabilities at each time step are needed. Even then, (3) is very computationally expensive to enforce as a constraint, so it is common to apply Boole's Inequality² to upper bound (2) with the sum of the marginal probabilities [2], [24], [26]:

$$\mathbb{P}\left(\bigcup_{t=1}^T \{Q(\mathbf{a}_t^*) \leq 1\}\right) \leq \sum_{i=1}^T \mathbb{P}(Q(\mathbf{a}_i^*) \leq 1) \quad (4)$$

Boole's Inequality, however, is a very conservative upper bound and also introduces the undesirable phenomenon of finer discretizations across time producing higher risk. We note that once upper bounds on the marginal probabilities are established, one can simply enforce a risk bound along the entire trajectory by constraining the sum of the marginal upper bounds if desired.

D. The cc-MPC Problem

In this paper, we derive results for the cc-MPC problem defined below.

$$\min_{\mathbf{x}_{1:T}, \mathbf{u}_{0:T}} c(\mathbf{x}_{1:T}, \mathbf{u}_{1:T}) \quad (5a)$$

$$\mathbf{x}_{t+1} = f(\mathbf{x}_t, \mathbf{u}_t), \quad t \in [T-1] \quad (5b)$$

$$\mathbb{P}(Q(\mathbf{a}_t^*) \leq 1) \leq \epsilon, \quad t \in [T] \quad (5c)$$

$$\mathbf{u}_{min} \leq \mathbf{u}_t \leq \mathbf{u}_{max}, \quad t \in [T] \quad (5d)$$

$$\mathbf{x}_{min} \leq \mathbf{x}_t \leq \mathbf{x}_{max}, \quad t \in [T] \quad (5e)$$

Where \mathbf{x}_t is the state vector, \mathbf{u}_t is the control vector, c is some cost function, f is a discrete time system modeling ego vehicle dynamics, \mathbf{u}_{min} and \mathbf{u}_{max} are control limits and \mathbf{x}_{min} and \mathbf{x}_{max} are state limits. We assume that the ego vehicle dynamics are deterministic as modern feedback control systems for autonomous vehicles are effective at tracking trajectories with positional error on the order of ten centimeters [14], [34]. Thus, the only difference between this problem and standard deterministic MPC formulations is the chance constraint (5c) which ensures that the probability of the vehicle colliding with an agent is no more than ϵ at each time step. Enforcing this chance-constraint will be the focus of Section IV.

IV. ENFORCING THE NON-GAUSSIAN CHANCE-CONSTRAINT

In this section, we show how the chance-constraint (5c) can be enforced with deterministic nonlinear constraints. While the resulting constraints are nonlinear and non-convex, they are differentiable, and our numerical experiments in Section VI show that solvers generated with FORCES Pro can handle these constraints very effectively [10]. Subsection IV-A begins by showing that upper bounds on the probability of violating constraints that are defined as the sub-level

²Boole's Inequality can actually be seen as the Inclusion-Exclusion principle with only sets of cardinality one in $\mathcal{P}([T])$ used.

sets of polynomial functions in random vectors can be established using Cantelli's Inequality. As a consequence, an upper bound can be established on risk (5c) with the first four moments of \mathbf{a}_t^* at each time step. Since \mathbf{a}_t^* is the agents position in the planned ego vehicle coordinates, its distribution changes as a function of the state variables in the optimization problem. Subsection IV-B addresses this issue. Section IV-C then shows how mixture models should be handled.

A. Bounding Risk with Cantelli's Inequality

We begin with a general formulation that is valid for all constraints defined as the sub-level set of polynomials $g : \mathbb{R}^n \rightarrow \mathbb{R}$ in n dimensional random vectors \mathbf{w} before showing how it applies to our case. As a simple consequence of Cantelli's Inequality [13], also known as the one-tailed Chebyshev Inequality, we have:

$$\mathbb{P}(g(\mathbf{w}) \leq 0) \begin{cases} \leq \frac{\text{Var}[g(\mathbf{w})]}{\text{Var}[g(\mathbf{w})] + \mathbb{E}[g(\mathbf{w})]^2} & \mu_{g(\mathbf{w})} \geq 0 \\ \geq 1 - \frac{\text{Var}[g(\mathbf{w})]}{\text{Var}[g(\mathbf{w})] + \mathbb{E}[g(\mathbf{w})]^2} & \mu_{g(\mathbf{w})} < 0 \end{cases} \quad (6)$$

The expression in the case $\mu_{g(\mathbf{w})} \geq 0$ will be denoted by $\text{Cant}(g(\mathbf{w}))$ for brevity. Thus, the risk can be upper bounded in the case that $\mu_{g(\mathbf{w})} \geq 0$. We note that this is not a particularly restrictive requirement as $\mu_{g(\mathbf{w})} < 0$ usually corresponds to relatively "high risk" scenarios. Analytically, this can be seen as the Cantelli bound provides a loose lower bound on the risk. It also intuitively makes sense as $\mu_{g(\mathbf{w})} < 0$ means the average case involves constraint violation. An important property of g being a polynomial is that the n_{th} moment of $g(\mathbf{w})$, i.e. $\mathbb{E}[g(\mathbf{w})^n]$, can be computed as the weighted sum of moments of \mathbf{w} . This is true because $g(\mathbf{w})^n$ is, itself, a polynomial to which the linearity of expectation can be applied. This fact is stated more formally in Proposition 1. In practice, the multi-index and coefficient sets can be found using symbolic algebra.

Proposition 1. *For any n dimensional random vector \mathbf{w} , any polynomial $g \in \mathbb{R}[\mathbf{w}]$ and any $m \in \mathbb{N}$, there exists a set of multi-indices $\mathcal{A} \subset \mathbb{N}^n$ and coefficients $C_{\mathcal{A}} = \{c_{\alpha} \in \mathbb{R} : \alpha \in \mathcal{A}\}$ s.t.:*

$$\mathbb{E}[g(\mathbf{w})^m] = \sum_{\alpha \in \mathcal{A}} c_{\alpha} \mathbb{E}[\mathbf{w}^{\alpha}] \quad (7)$$

Proof. Since g is a polynomial, $g(\mathbf{w})^n$ is also a polynomial in \mathbf{w} since $\mathbb{R}[\mathbf{w}]$ is closed under multiplication. Thus, we have the existence of \mathcal{A} and $C_{\mathcal{A}}$ s.t. $g(\mathbf{w})^n = \sum_{\alpha \in \mathcal{A}} c_{\alpha} \mathbf{w}^{\alpha}$. Applying the expectation operator to both sides and the linearity of expectation, we arrive at the result. \square

For our problem, since $Q(\mathbf{a}_t^*)$ is a second order polynomial in \mathbf{a}_t^* , Proposition 1 applies. Since we need the variance of $Q(\mathbf{a}_t^*)$, which is the second central moment, to apply the Cantelli bound, we will ultimately need the fourth order moments of \mathbf{a}_t^* . By the Cantelli bound, we can enforce the following constraints to ensure the chance-constraints are

satisfied:

$$\frac{\text{Var}[Q(\mathbf{a}_t^*)]}{\text{Var}[Q(\mathbf{a}_t^*)] + \mathbb{E}[Q(\mathbf{a}_t^*) - 1]^2} \leq \epsilon \quad (8)$$

$$\mathbb{E}[Q(\mathbf{a}_t^*) - 1] \geq 0 \quad (9)$$

Note that $\text{Var}[Q(\mathbf{a}_t^*)] = \text{Var}[Q(\mathbf{a}_t^*) - 1]$ since the variance of a random variable is translation invariant.

B. Transforming Coordinates

One major challenge is that the moments of $Q(\mathbf{a}_t^*)$ change as a function of the ego vehicle position $\mathbf{y}_t = [x_t, y_t]^T$ and heading θ_t since \mathbf{a}_t^* is related to the global frame random vector \mathbf{a}_t by:

$$\mathbf{a}_t^* = R(-\theta_t)(\mathbf{a}_t - \mathbf{y}_t) \quad (10)$$

Since \mathbf{y}_t and θ_t are decision variables in the optimization problem, the moments of $Q(\mathbf{a}_t^*)$ need to be expressed in the optimization problem as a function of \mathbf{y}_t and θ_t . We make the simplifying assumption that the distribution of \mathbf{a}_t conditioned on the planned ego vehicle trajectory is constant (i.e, the expected behavior of the agent does not change w.r.t. a different planned route for the ego vehicle). Instead of accounting for both the translation and rotation in the new moments, we instead define:

$$Q^t = R^T(-\theta_t)QR(-\theta_t) \quad (11)$$

$$\tilde{\mathbf{a}}_t = \mathbf{a}_t - \mathbf{y}_t \quad (12)$$

And since $Q(\mathbf{a}_t^*) = Q^t(\tilde{\mathbf{a}}_t)$, we instead only need to compute the moments of $\tilde{\mathbf{a}}_t$ and don't need to worry about accounting for the rotation when computing moments. The first moment of $Q(\mathbf{a}_t^*)$ has the simple closed form expression [25]:

$$\mathbb{E}[Q(\mathbf{a}_t^*)] = \text{Tr}[Q^t \Sigma_{\mathbf{a}_t}] + \mu_{\tilde{\mathbf{a}}_t}^T Q^t \mu_{\tilde{\mathbf{a}}_t} \quad (13)$$

Note that $\Sigma_{\mathbf{a}_t^*} = \Sigma_{\tilde{\mathbf{a}}_t}$ since the covariance matrix of a random vector is invariant under translation.

1) *Variance in the Gaussian Case:* In the Gaussian case, there exists the following solution for the variance of $Q(\tilde{\mathbf{a}}_t)$ in terms of $\mu_{\tilde{\mathbf{a}}_t}$ and $\Sigma_{\mathbf{a}_t}$ [28]:

$$\text{Var}[Q(\mathbf{a}_t^*)] = 2\text{Tr}[Q^t \Sigma_{\mathbf{a}_t} Q^t \Sigma_{\mathbf{a}_t}] + 4\mu_{\tilde{\mathbf{a}}_t}^T Q^t \Sigma_{\mathbf{a}_t} Q^t \mu_{\tilde{\mathbf{a}}_t} \quad (14)$$

2) *Variance in the Non-Gaussian Case:* In the non-Gaussian case, higher order moments will be needed to determine the variance of $Q(\mathbf{a}_t^*)$. Since equation (13) applies to the non-Gaussian case as well, we can focus on determining the second moment of $Q(\mathbf{a}_t^*)$ to determine its variance. Letting $\{x, y\}^4$ denote the fourth cartesian power of the set $\{x, y\}$, we can apply an alternate representation of the quadratic form to arrive at the second moment:

$$\mathbb{E}[Q^t(\tilde{\mathbf{a}}_t)^2] = \sum_{(i,j,k,l) \in \{x,y\}^4} Q_{ij}^t Q_{kl}^t \mathbb{E}[\tilde{a}_{i_t} \tilde{a}_{j_t} \tilde{a}_{k_t} \tilde{a}_{l_t}] \quad (15)$$

Thus, we see that the second moment of the quadratic form can be determined with the fourth order moments of $\tilde{\mathbf{a}}_t$. More precisely, it can be determined with moments of the form:

$$\mathbb{E}[\tilde{a}_{x_t}^n \tilde{a}_{y_t}^m] = \mathbb{E}[(a_{x_t} - x_t)^n (a_{y_t} - y_t)^m] \quad (16)$$

Where $m + n = 4$. By applying the multi-binomial theorem, we have that:

$$\mathbb{E}[(a_{x_t} - x_t)^n (a_{y_t} - y_t)^m] = \quad (17)$$

$$\sum_{k_1=0}^n \sum_{k_2=0}^m n_{k_1} m_{k_2} (-x_t)^{n-k_1} (-y_t)^{m-k_2} \mathbb{E}[a_{x_t}^{k_1} a_{y_t}^{k_2}] \quad (18)$$

Where n_{k_1}, m_{k_2} are binomial coefficients. Thus, we have that $\mathbb{E}[Q^t(\tilde{\mathbf{a}}_t)^2]$ can ultimately be expressed in terms of all of the moments of \mathbf{a}_t up to order four. In practice, symbolic algebra can be used to reduce the number of terms in equation (14) and the binomial coefficients of equation (18) can be computed *a priori*.

C. Handling Mixture Models

In this subsection, we discuss how chance-constraints should be enforced in the case that \mathbf{a}_t are mixture models with n components \mathbf{a}_{i_t} and weights w_i . We begin by noting that all results presented thus far have been for general random vectors with known moments up to order four, so they apply directly to mixture models with known moments as well. Theorem 2 and Corollary 3 show that the moments of mixture models are equivalent to the weighted sum of the moments of their components. Thus, we can simply compute the moments of \mathbf{a}_t as the weighted sum of those of its components prior to the optimization, essentially treating the mixture model in the same way we would treat an uni-modal distribution. The resulting optimization problem would have the same size as the unimodal case, which is desirable.

However, Theorem 4 indicates that we are likely to get tighter bounds if, instead, we enforce the Cantelli bound on each mixture component and constrain the weighted sum of the component Cantelli bounds:

$$\sum_{i=1}^n w_i \text{Cant}(Q(\mathbf{a}_{i_t}^*) \leq 1) \leq \epsilon \quad (19)$$

In practice, we find that enforcing the constraint (19) produces tighter bounds. In fact, applying a single Cantelli bound on the mixture model will be more conservative than (19) in almost all circumstances. Discussion on the conditions under which the inequality is strict is included in the appendix.

Theorem 2. *For any mixture model X with n components X_i with mixture weights w_i and any measurable function g , we have that $\mathbb{E}[g(X)] = \sum_{i=1}^n w_i \mathbb{E}[g(X_i)]$.*

Proof. By the Law of the Unconscious Statistician, we have (20a). By definition, the pdf of X is $f_X(x) = \sum_{i=1}^n w_i f_{X_i}(x)$ where f_{X_i} are the pdfs of X_i . Plugging that in and then interchanging the order of integration and summation, we arrive at the result.

$$\mathbb{E}[g(X)] = \int_{\mathbb{R}} g(x) f_X(x) dx \quad (20a)$$

$$= \int_{\mathbb{R}} g(x) \sum_{i=1}^n f_{X_i}(x) w_i dx \quad (20b)$$

$$= \sum_{i=1}^n w_i \int_{\mathbb{R}} g(x) f_{X_i}(x) dx \quad (20c)$$

$$= \sum_{i=1}^n w_i \mathbb{E}[g(X_i)] \quad (20d)$$

□

Corollary 3. For any mixture model X with n components X_i and mixture weights w_i , for any $m \in \mathbb{N}$, $\mathbb{E}[X^m] = \sum_{i=1}^n w_i \mathbb{E}[X_i^m]$

Proof. Substitute in $g(X) = X^m$ in Theorem 2. □

Theorem 4. For any random vector \mathbf{w} with n components w_i and weights w_i and any measurable function g , if $\mathbb{E}[g(\mathbf{w}_i)] > 0, \forall i \in [n]$, we have that:

$$\mathbb{P}(g(\mathbf{w}) \leq 0) \leq \sum_{i=1}^n w_i \text{Cant}(g(\mathbf{w}_i)) \quad (21a)$$

$$\leq \text{Cant}(g(\mathbf{w})) \quad (21b)$$

Proof. See appendix. □

V. APPLICATION TO TRAJECTORY PLANNING WITH MODEL PREDICTIVE CONTOURING CONTROL

In the context of autonomous driving, an approximate coarse-grained path is almost always available to trajectory planners as:

- 1) Most autonomous driving systems have maps of lane geometries *a priori*
- 2) Most autonomous driving systems have routers and higher level planners that provide a coarse plan (e.g: a sequence of waypoints along the road).

This availability of a “reference path” makes model predictive contouring control (MPCC) an effective solution for trajectory planning. MPCC is a methodology for expressing an approximation of the minimum distance from a point to a third order polynomial in closed form. This allows for deviations from the reference path to be included in the cost function of an optimization problem. By jointly applying MPCC and our chance-constraint formulation, we arrive at a trajectory planner that can find trajectories with low deviation from the reference path while satisfying some desired level of safety. As shown in the experiments section, this allows for rich qualitative behavior to be generated. In the following subsections, we present a brief overview of the MPCC formulation we use for numerical experiments; the interested reader is referred to [21], [32] for additional details. For the dynamics model, we propose using the kinematic bicycle model, but note that other dynamics model may easily be substituted instead.

A. Reference Path

Following the standard contouring control formulation, the reference path is represented as third order polynomials in

an arc-length parameter $s \in [0, L]$ where L is the length of the path:

$$\begin{bmatrix} x_{ref}(s) \\ y_{ref}(s) \end{bmatrix} = \begin{bmatrix} c_{x0} + c_{x1}s + c_{x2}s^2 + c_{x3}s^3 \\ c_{y0} + c_{y1}s + c_{y2}s^2 + c_{y3}s^3 \end{bmatrix} \quad (22)$$

Where c_{xi} and c_{yi} for $i \in [3]$ are the polynomial coefficients. We note that parameterizing a third order polynomial path with arc-length is a difficult problem itself without exact solutions, but approximation methods are well-studied [11], [12], [27]. For our experiments, we applied a simple approximation by initially generating the polynomials with $s \in [0, 1]$ and then the lengths of the polynomials were computed by numerical integration. The coefficients are then scaled s.t. $s \in [0, L]$. The heading at each point on the reference path, denote it $\Theta(s)$, can be expressed in terms of the derivatives of the polynomials:

$$\Theta(s) = \arctan \left(\frac{\partial y_{ref}}{\partial x_{ref}}(s) \right) \quad (23)$$

B. Contouring Deviation and Lag Error

Ideally, the Euclidean distance from the ego vehicle to the nearest point on the reference path, which we will refer to as *contouring deviation*³, would be used as the measure of deviation from the reference path, but doing so requires a minimization over the path parameter s that is computationally intractable to perform in an optimization routine. The standard solution is to approximate the contouring deviation by using the distance the vehicle has travelled, denote it Δ , as an approximation. This only requires adding an additional integrator variable to the dynamics model as the time derivative of Δ is the vehicles speed. Letting $\bar{x}_t = x_t - x_{ref}(\Delta_t)$ and $\bar{y}_t = y_t - y_{ref}(\Delta_t)$, contouring deviation can be approximated with:

$$D_t = \sin(\Theta(\Delta_t))\bar{x}_t - \cos(\Theta(\Delta_t))\bar{y}_t \quad (24)$$

It is also important to penalize error between Δ and the true parameter corresponding to the closest point on the path to the vehicle. This quantity is known as the *lag error* and can be approximated by:

$$L_t = -\cos(\Theta(\Delta_t))\bar{x}_t - \sin(\Theta(\Delta_t))\bar{y}_t \quad (25)$$

C. Ego Vehicle Model

For driving in nominal conditions, the kinematic bicycle model is known to provide a high level of fidelity while requiring less computational cost than a dynamics model; thus it is well suited for trajectory planning [20]. The state of the vehicle is defined as $\mathbf{x} = [x, y, \theta, v, \delta, \Delta]^T$ where x, y denotes the vehicle’s position and θ denotes the heading in the global coordinates. v denotes speed, δ denotes the front steering angle, and Δ denotes the distance travelled; its relevance was explained in Subsection V-B. The control inputs are $\mathbf{u} = [u_a, u_\delta]^T$ where u_a is acceleration and u_δ is the rate of change of the steering angle. The relevant physical

³In the literature, this is usually known as *contouring error*, but we call it contouring deviation as deviation from the reference path to satisfy chance-constraints is not necessarily undesirable.

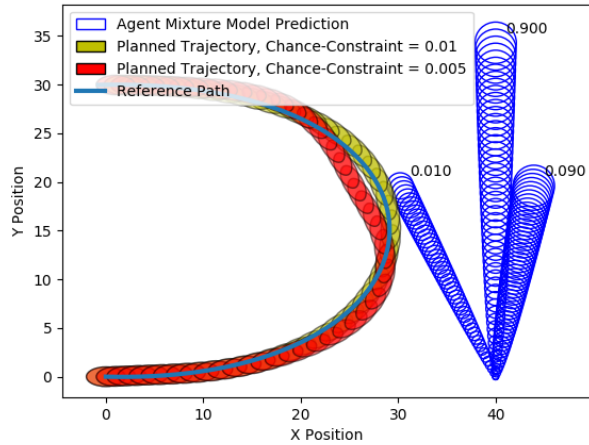


Fig. 2. Example of two ego vehicle trajectories planned with different chance-constraints. A three component mixture model prediction is shown in blue with their corresponding mixture weights. The size of the prediction ellipses correspond to the moment-matched 99% confidence regions for multivariate Gaussians.

parameters of the vehicle in this model are the distances from the center of gravity to the front and rear axles; we denote them l_f and l_r respectively. The continuous time model is thus:

$$\dot{\mathbf{x}} = \begin{bmatrix} v \cos(\theta + \beta) \\ v \sin(\theta + \beta) \\ \frac{v}{l_r} \sin(\beta) \\ u_a \\ u_\delta \\ v \end{bmatrix} \quad (26)$$

Where β is the side-slip angle at the vehicles center of gravity and is a function of the steer angle:

$$\beta = \arctan\left(\frac{l_r}{l_f + l_r} \tan(\delta)\right) \quad (27)$$

VI. NUMERICAL EXPERIMENTS

For numerical experiments, we used optimizers generated with FORCES Pro on a desktop with an Intel Core i9-7980XE CPU clocked at 2.60 GHz. FORCES Pro is a software package that generates high performance interior-point solvers for optimal control problems that exploit structure induced in the Karush-Kuhn-Tucker (KKT) system by the step-wise nature of optimal control problems [10], [35]. A third order polynomial path emulating a U-turn was generated to serve as the reference path. Fake non-Gaussian behavior predictions were created by manually specifying mean vectors and covariance matrices, computing the higher order moments corresponding to multivariate Gaussians with these parameters, and then perturbing the higher order moments. In the cost function, we penalize contouring deviation, lag error, control effort, and deviation from a reference speed (e.g: the roads speed limit):

$$\sum_{t=1}^T c_D D_t^2 + c_L L_t^2 + \mathbf{u}_t^T R \mathbf{u}_t + c_v (v_t - v_{ref})^2 \quad (28)$$

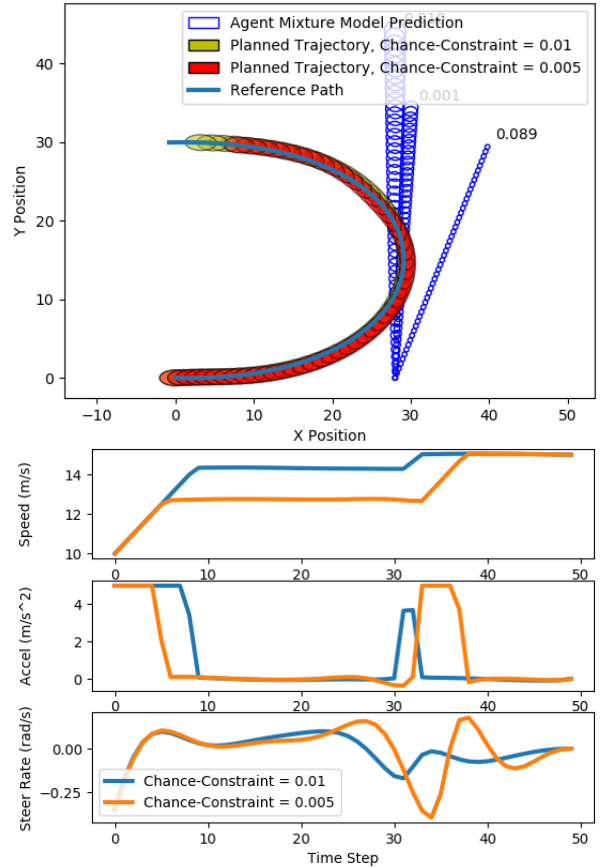


Fig. 3. (Top): Plot of the reference path, resulting planned trajectories, and agent predictions. (Bottom): Plot of the vehicle speed profile and control inputs.

Where c_D, c_L, c_v and $R \in \mathcal{S}_{++}^2$ are cost function parameters and v_{ref} is the reference speed. 50 time steps were used with intervals of 0.1 seconds for a planning horizon of 5 seconds. The continuous time dynamics were discretized with the explicit fourth order Runge-Kutta (RK4) method. We denote the resulting discrete time system as:

$$\mathbf{x}_{t+1} = f_{RK4}(\mathbf{x}_t, \mathbf{u}_t) \quad (29)$$

Initial guesses for the optimizer were produced by simulating the system (29) with zero control inputs.

A. Results for Two Scenarios

Figure 2 shows two trajectories planned with different chance-constraints. While a chance-constraint of 0.01 allows for the vehicle to follow the reference path exactly, the vehicle has to deflect about a meter off the reference path to satisfy a chance-constraint of 0.005. Figure 3 shows a scenario where the agent crosses the ego vehicle reference path for a short duration while the reference speed for the ego vehicle is 15 m/s. In the case that the chance-constraint for the planner is set more conservatively, we see that a slower speed profile is planned to allow for the other vehicle to

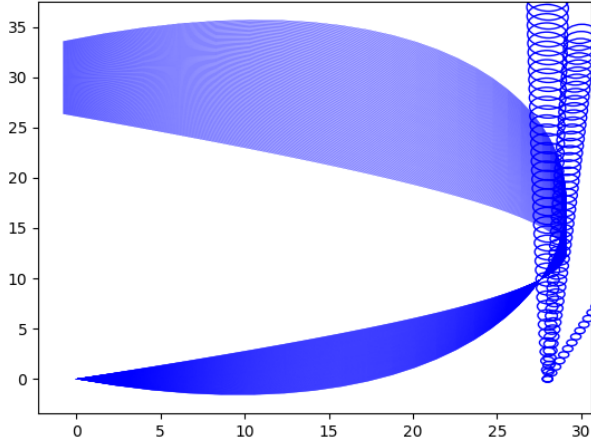


Fig. 4. 200 paths tested with a constant behavior prediction.

pass with a greater distance from the ego vehicle. In both scenarios shown, the optimizer arrives at a local optimum in less than 20 ms.

B. Testing Reliability

To test the reliability of the planner, in the scenario shown in Figure 3, the parameters of the reference path were perturbed to generate the 200 different paths shown in Figure 4. The trajectory planner was tested on all 200 paths with a chance-constraint of 0.01. 100% of the trials successfully achieved a local optima with a mean solve time of 15.4 ms and a worst case solve time of 21.1 ms with the KKT conditions satisfied within numerical tolerances.

VII. CONCLUSIONS

In this paper, we presented a chance-constrained MPC formulation for autonomous vehicles that can handle mixtures of non-Gaussian distributions of agent positions. We then demonstrated that it can be applied to the problem of chance-constrained trajectory planning in a model predictive contouring control formulation. While the deterministic constraints that imply the chance-constraints in the resulting NLP are nonlinear and non-convex, they are differentiable, and state-of-the-art interior point solvers generated with FORCES Pro can easily find local optima in real-time. We note that while enforcing chance-constraints using the Cantelli bound provides great generality, this generality can also produce excessively conservative results. Future works should consider leveraging higher order moments, or other distribution specific information, to establish tighter bounds.

VIII. APPENDIX

Lemma 5. *The function $\phi(x, y) = \frac{x^2}{y}$ on the domain $x \in \mathbb{R}$ and $y > 0$ is convex.*

Proof. It is sufficient for the Hessian of ϕ to be positive semi-definite. The Hessian of ϕ is:

$$H_\phi(x, y) = \begin{bmatrix} 2y^{-1} & -2xy^{-2} \\ -2xy^{-2} & 2x^2y^{-3} \end{bmatrix} \quad (30)$$

Its eigenvalues can be found in closed form and are:

$$\lambda_1 = 0 \quad \lambda_2 = 2(x^2 + y^2)y^{-3} \quad (31)$$

Since $y > 0$ on the domain of ϕ , both eigenvalues are non-negative, so the Hessian is positive semi-definite on the domain of ϕ . \square

A. Proof of Theorem 4

Proof. We begin by showing the inequality (21a). The probability of constraint violation can be written as the expectation of the indicator function. Define the indicator function:

$$\mathbb{1}_{(-\infty, 0]}(x) = \begin{cases} 1 & x \in (-\infty, 0] \\ 0 & o.w. \end{cases} \quad (32)$$

The probability of constraint violation can then be expressed as:

$$\mathbb{P}(g(\mathbf{w}) \leq 0) = \mathbb{E}[\mathbb{1}_{(-\infty, 0]}(g(\mathbf{w}))] \quad (33)$$

The indicator function (32) is measurable because indicator functions are measurable i.f.f. the set they are defined on is measurable, and $(-\infty, 0]$ is measurable because it's a Borel set [16]. Furthermore, the composition of measurable functions is measurable, so we can apply Theorem 2:

$$\mathbb{E}[\mathbb{1}_{(-\infty, 0]}(g(\mathbf{w}))] = \sum_{i=1}^n w_i \mathbb{E}[\mathbb{1}_{(-\infty, 0]}(g(\mathbf{w}_i))] \quad (34)$$

$$= \sum_{i=1}^n w_i \mathbb{P}(g(\mathbf{w}_i) \leq 0) \quad (35)$$

$$\leq \sum_{i=1}^n w_i \text{Cant}(g(\mathbf{w}_i)) \quad (36)$$

Now, we show the inequality (21b). Begin by noting that:

$$\frac{\text{Var}[g(\mathbf{w})]}{\text{Var}[g(\mathbf{w})] + \mathbb{E}[g(\mathbf{w})]^2} = 1 - \frac{\mu_{g(\mathbf{w})}^2}{\mathbb{E}[g(\mathbf{w})^2]} \quad (37)$$

$$= 1 - \phi(\mu_{g(\mathbf{w})}, \mathbb{E}[g(\mathbf{w})^2]) \quad (38)$$

By Lemma 5, ϕ above is convex since $\mathbb{E}[g(\mathbf{w})^2] > 0$ by definition⁴. Furthermore, by Corollary 3, we have that:

$$\left[\frac{\mu_{g(\mathbf{w})}}{\mathbb{E}[g(\mathbf{w})^2]} \right] = \sum_{i=1}^n w_i \left[\frac{\mu_{g(\mathbf{w}_i)}}{\mathbb{E}[g(\mathbf{w}_i)^2]} \right] \quad (39)$$

Thus, by the finite version of Jensen's Inequality [31]:

$$\phi(\mu_{g(\mathbf{w})}, \mathbb{E}[g(\mathbf{w})^2]) \leq \sum_{i=1}^n w_i \phi(\mu_{g(\mathbf{w}_i)}, \mathbb{E}[g(\mathbf{w}_i)^2]) \quad (40)$$

Subtracting the left hand side quantity from 1 and the right hand side quantity from $\sum_{i=1}^n w_i = 1$, we have:

$$\text{Cant}(g(\mathbf{w})) \geq \sum_{i=1}^n w_i (1 - \phi(\mu_{g(\mathbf{w}_i)}, \mathbb{E}[g(\mathbf{w}_i)^2])) \quad (41)$$

$$= \sum_{i=1}^n w_i \text{Cant}(g(\mathbf{w}_i)) \quad (42)$$

\square

⁴Technically, it is possible for the second moment to be zero when the random variable is zero with probability one, but this is a pathological case that should never be encountered in practice.

B. The Strictness of Inequality (21b)

Note that if the inequality (40) is strict, then we will have that inequality (21b) is strict as well. If ϕ is strictly convex, then Jensen's Inequality becomes strict except when all the arguments of ϕ are equal for each component in the summation [8]. A sufficient condition for strict convexity is that the Hessian of ϕ is positive definite which is not satisfied. However, because the first eigenvalue is zero but the second eigenvalue is strictly positive, quadratic forms in H_ϕ are strictly positive on \mathbb{R}^2 except the line corresponding to the first eigenvector of H_ϕ . If we restrict the domain of ϕ to not include this line, we have strict convexity of ϕ and thus (40) and (21b) become strict.

REFERENCES

- [1] Brian Axelrod, Leslie Pack Kaelbling, and Tomás Lozano-Pérez. Provably safe robot navigation with obstacle uncertainty. *The International Journal of Robotics Research*, 37(13-14):1760–1774, 2018.
- [2] Lars Blackmore and Masahiro Ono. Convex chance constrained predictive control without sampling. In *AIAA Guidance, Navigation, and Control Conference*, page 5876, 2009.
- [3] Lars Blackmore, Masahiro Ono, Askar Bektassov, and Brian C Williams. A probabilistic particle-control approximation of chance-constrained stochastic predictive control. *IEEE transactions on Robotics*, 26(3):502–517, 2010.
- [4] Giuseppe C Calafiore and Marco C Campi. The scenario approach to robust control design. *IEEE Transactions on automatic control*, 51(5):742–753, 2006.
- [5] Giuseppe Carlo Calafiore and Laurent El Ghaoui. On distributionally robust chance-constrained linear programs. *Journal of Optimization Theory and Applications*, 130(1):1–22, 2006.
- [6] Yuning Chai, Benjamin Sapp, Mayank Bansal, and Dragomir Anguelov. Multipath: Multiple probabilistic anchor trajectory hypotheses for behavior prediction. *arXiv preprint arXiv:1910.05449*, 2019.
- [7] Henggang Cui, Thi Nguyen, Fang-Chieh Chou, Tsung-Han Lin, Jeff Schneider, David Bradley, and Nemanja Djuric. Deep kinematic models for physically realistic prediction of vehicle trajectories. *arXiv preprint arXiv:1908.00219*, 2019.
- [8] Zdravko Cvetkovski. Convexity, jensen's inequality. In *Inequalities*, pages 69–77. Springer, 2012.
- [9] Nachiket Deo and Mohan M Trivedi. Multi-modal trajectory prediction of surrounding vehicles with maneuver based lstms. In *2018 IEEE Intelligent Vehicles Symposium (IV)*, pages 1179–1184. IEEE, 2018.
- [10] Alexander Domahidi and Juan Jerez. Forces professional. embotech gmbh (<http://embotech.com/forces-pro>). July, 2014.
- [11] Kaan Erkorkmaz and Yusuf Altintas. Quintic spline interpolation with minimal feed fluctuation. *J. Manuf. Sci. Eng.*, 127(2):339–349, 2005.
- [12] MS Floater. Arc length estimation and the convergence of polynomial curve interpolation. *BIT Numerical Mathematics*, 45(4):679–694, 2005.
- [13] Yacov Y Haimes and Ralph E Steuer. *Research and Practice in Multiple Criteria Decision Making: Proceedings of the XIVth International Conference on Multiple Criteria Decision Making (MCDM) Charlottesville, Virginia, USA, June 8–12, 1998*, volume 487. Springer Science & Business Media, 2012.
- [14] Gabriel M Hoffmann, Claire J Tomlin, Michael Montemerlo, and Sebastian Thrun. Autonomous automobile trajectory tracking for off-road driving: Controller design, experimental validation and racing. In *2007 American Control Conference*, pages 2296–2301. IEEE, 2007.
- [15] Joey Hong, Benjamin Sapp, and James Philbin. Rules of the road: Predicting driving behavior with a convolutional model of semantic interactions. In *Proceedings of the IEEE Conference on Computer Vision and Pattern Recognition*, pages 8454–8462, 2019.
- [16] John K Hunter. Measure theory. *University Lecture Notes, Department of Mathematics, University of California at Davis*. http://www.math.ucdavis.edu/~hunter/measure_theory, 2011.
- [17] Ashkan Jasour and Brian Williams. Sequential chance optimization for flow-tube based control of probabilistic nonlinear systems. *arXiv preprint arXiv:1912.03572*, 2019.
- [18] Ashkan M Jasour, Andreas Hofmann, and Brian C Williams. Momentum-of-squares approach for fast risk estimation in uncertain environments. In *2018 IEEE Conference on Decision and Control (CDC)*, pages 2445–2451. IEEE, 2018.
- [19] Ashkan M Jasour and Brian C Williams. Risk contours map for risk bounded motion planning under perception uncertainties. *Robot.; Sci. and Syst.*, 2019.
- [20] Jason Kong, Mark Pfeiffer, Georg Schilb, and Francesco Borrelli. Kinematic and dynamic vehicle models for autonomous driving control design. In *2015 IEEE Intelligent Vehicles Symposium (IV)*, pages 1094–1099. IEEE, 2015.
- [21] Denise Lam, Chris Manzie, and Malcolm C Good. Model predictive control for biaxial systems. *IEEE Transactions on Control Systems Technology*, 21(2):552–559, 2012.
- [22] Namhoon Lee, Wongun Choi, Paul Vernaza, Christopher B Choy, Philip HS Torr, and Manmohan Chandraker. Desire: Distant future prediction in dynamic scenes with interacting agents. In *Proceedings of the IEEE Conference on Computer Vision and Pattern Recognition*, pages 336–345, 2017.
- [23] Brandon Luders, Mangal Kothari, and Jonathan How. Chance constrained rrt for probabilistic robustness to environmental uncertainty. In *AIAA guidance, navigation, and control conference*, page 8160, 2010.
- [24] Yudong Ma, Sergey Vichik, and Francesco Borrelli. Fast stochastic mpc with optimal risk allocation applied to building control systems. In *2012 IEEE 51st IEEE Conference on Decision and Control (CDC)*, pages 7559–7564. IEEE, 2012.
- [25] Arakaparampil M Mathai and Serge B Provost. *Quadratic forms in random variables: theory and applications*. Dekker, 1992.
- [26] Masahiro Ono and Brian C Williams. Iterative risk allocation: A new approach to robust model predictive control with a joint chance constraint. In *2008 47th IEEE Conference on Decision and Control*, pages 3427–3432. IEEE, 2008.
- [27] John W Peterson. Arc length parameterization of spline curves. <https://saccade.com/writing/graphics/RE-PARAM.PDF>.
- [28] Alvin C Rencher and G Bruce Schaalje. *Linear models in statistics*. John Wiley & Sons, 2008.
- [29] Venkatraman Renganathan, Iman Shames, and Tyler H Summers. Towards integrated perception and motion planning with distributionally robust risk constraints. *arXiv preprint arXiv:2002.02928*, 2020.
- [30] Nicholas Rhinehart, Kris M Kitani, and Paul Vernaza. R2P2: A reparameterized pushforward policy for diverse, precise generative path forecasting. In *Proceedings of the European Conference on Computer Vision (ECCV)*, pages 772–788, 2018.
- [31] Jamal Rooi. Some refinements of discrete jensen's inequality and some of its applications. *arXiv preprint math/0610736*, 2006.
- [32] Wilko Schwarting, Javier Alonso-Mora, Liam Pauli, Sertac Karaman, and Daniela Rus. Parallel autonomy in automated vehicles: Safe motion generation with minimal intervention. In *2017 IEEE International Conference on Robotics and Automation (ICRA)*, pages 1928–1935. IEEE, 2017.
- [33] Tyler Summers. Distributionally robust sampling-based motion planning under uncertainty. In *2018 IEEE/RSJ International Conference on Intelligent Robots and Systems (IROS)*, pages 6518–6523. IEEE, 2018.
- [34] Junmin Wang, Joe Steiber, and Bapiraju Surampudi. Autonomous ground vehicle control system for high-speed and safe operation. In *2008 American Control Conference*, pages 218–223. IEEE, 2008.
- [35] Andrea Zanelli, Alexander Domahidi, J Jerez, and Manfred Morari. Forces nlp: an efficient implementation of interior-point methods for multistage nonlinear nonconvex programs. *International Journal of Control*, 93(1):13–29, 2020.
- [36] Bingyu Zhou, Wilko Schwarting, Daniela Rus, and Javier Alonso-Mora. Joint multi-policy behavior estimation and receding-horizon trajectory planning for automated urban driving. In *2018 IEEE International Conference on Robotics and Automation (ICRA)*, pages 2388–2394. IEEE, 2018.